BIOCHEMISTRY
including biophysical chemistry & molecular biology

Article

pubs.acs.org/biochemistry

Quinine Binding by the Cocaine-Binding Aptamer. Thermodynamic and Hydrodynamic Analysis of High-Affinity Binding of an Off-Target Ligand

Oren Reinstein,[†] Mina Yoo,[†] Chris Han,[†] Tsering Palmo,[†] Simone A. Beckham,[§] Matthew C. J. Wilce,[§] and Philip E. Johnson*[,†]

[†]Department of Chemistry, York University, 4700 Keele Street, Toronto, Ontario, Canada M3J 1P3

[§]Department of Biochemistry and Molecular Biology, Monash University, Wellington Road, Clayton, Victoria 3800, Australia

Supporting Information

ABSTRACT: The cocaine-binding aptamer is unusual in that it tightly binds molecules other than the ligand it was selected for. Here, we study the interaction of the cocaine-binding aptamer with one of these off-target ligands, quinine. Isothermal titration calorimetry was used to quantify the quinine-binding affinity and thermodynamics of a set of sequence variants of the cocaine-binding aptamer. We find that the affinity of the cocaine-binding aptamer for quinine is 30–40 times stronger than it is for cocaine. Competitive-binding studies demonstrate that both quinine and cocaine bind at the same site on the aptamer. The ligand-induced structural-switching binding mechanism of an aptamer variant that contains three base pairs in stem 1 is retained with quinine as a ligand. The short stem 1 aptamer is unfolded or loosely folded in the free form and becomes folded when bound to quinine. This folding is confirmed by NMR spectroscopy and by the short stem 1 construct having a more negative change in heat capacity of quinine binding than is seen when stem 1 has six base pairs. Small-angle X-ray scattering (SAXS) studies of the free aptamer and both the quinine- and the cocaine-bound forms show that, for the long stem 1 aptamers, the three forms display similar hydrodynamic properties, and the ab initio shape reconstruction structures are very similar. For the short stem 1 aptamer there is a greater variation among the SAXS-derived ab initio shape reconstruction structures, consistent with the changes expected with its structural-switching binding mechanism.

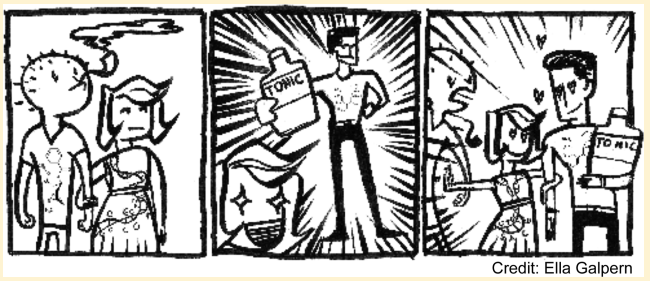

Credit: Ella Galpern

The past three decades have shown an increasing interest in aptamers due to their use in biosensor applications, nanowire assemblies, and pharmaceutical applications.[1−8] The growing demand and popularity of aptamers are partly due to the method with which they are generated. Through an in vitro selection process known as systematic evolution of ligands through exponential enrichment (SELEX), aptamers have the potential to acquire extremely high specificity and affinity for targets that can range from small molecules to entire cells.[9,10] Many methods of detection such as fluorescence, colorimetric, and electrochemical signals have been coupled with aptamer−ligand interactions to indicate the presence of an analyte. To produce the maximum desired signal, and therefore the greatest sensitivity, ligand binding has been coupled with structural changes in aptamers that result in the generation of detectable signals.[2] This ligand-dependent structural change is also referred to as a structural-switching mechanism. A particularly well-characterized system for the development of biosensors employing a structural-switching mechanism is that of the cocaine-binding aptamer.[11] The cocaine-binding aptamer has served as a model system for numerous biosensor applications[12−26] as well as for studies focused on supramolecular and nanotechnology applications. Many of these applications take advantage of the structural-switching binding mechanism that occurs with cocaine binding.[27−29]

The cocaine-binding aptamer is a DNA aptamer that is composed of three stems arranged around a three-way junction (Figure 1).[30,31] When stem 1 is shortened to three base pairs, the free aptamer (Figure 1, MN19) is unfolded or loosely folded and only becomes structured when it binds its target ligand.[31,32] In contrast, when stem 1 is longer (Figure 1, MN4), the aptamer has its secondary structure formed in the free form, and no large-scale structural change occurs when the aptamer binds cocaine.[31] This stem-length dependence in the binding mechanism is retained when the DNA sequence is modified to favor the binding of deoxycholic acid and not cocaine.[33,34] In a variation of this structural-switching mechanism, the aptamer can also be split into two or three separate DNA strands, with the annealing of the strands coupled with ligand binding.[26,35−37]

Received: July 25, 2013
Revised: October 29, 2013
Published: October 31, 2013

dx.doi.org/10.1021/bi4010039 | *Biochemistry* 2013, 52, 8652−8662

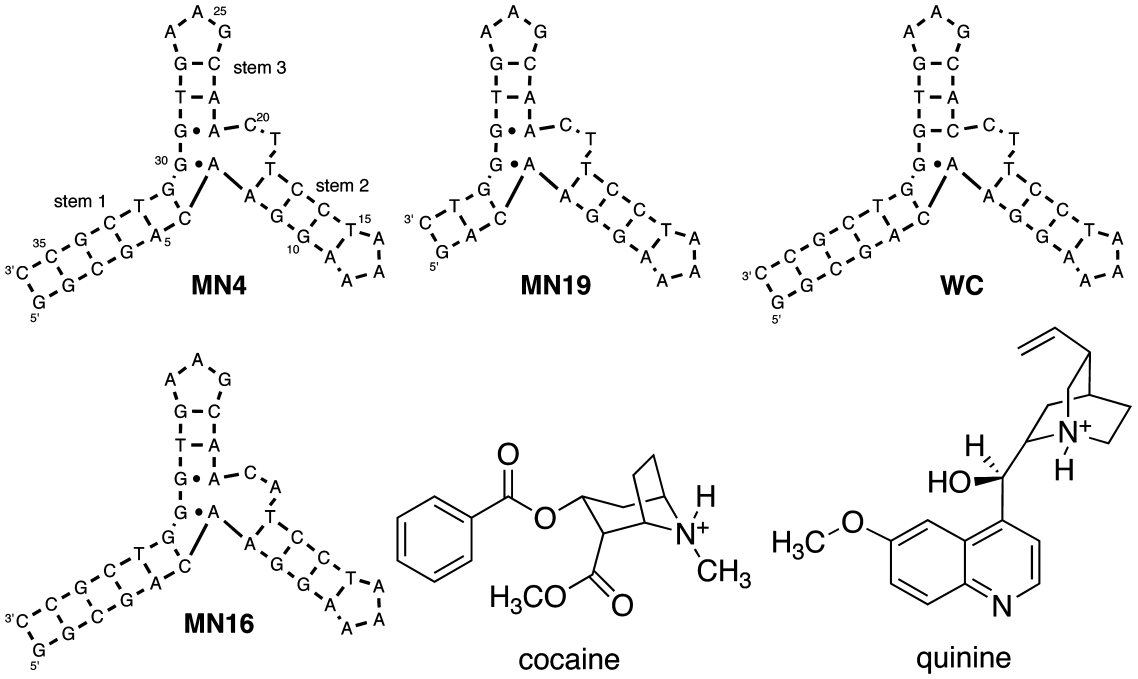

Figure 1. Sequence of the aptamer and chemical structure of ligands referred to in this study. Compared to MN4, aptamer MN19 has three base pairs removed from the end of stem 1. Aptamer WC contains a change at the three-way junction in which A21 has been replaced with a C, restoring the Watson–Crick base pair. MN16 is a weak-binding variant in which T19 has been swapped for an A. Dashes between nucleotides indicate Watson–Crick base pairs, and dots indicate non-Watson–Crick base pairs.

One feature of the cocaine-binding aptamer that sets it apart from other aptamers is its binding promiscuity. Though selected for cocaine binding, this aptamer also binds other alkaloids and even binds quinine with higher affinity than it binds cocaine.[38−40] Such versatility in ligand binding is uncommon among aptamers and is not a desirable characteristic for a biosensor, but it may be a useful property for the biotechnology applications of the cocaine-binding aptamer. The binding versatility of this aptamer leads to questions such as "How does the same sequence bind to different ligands?" and "Does the aptamer use the same binding site and binding mechanism for all ligands?" In this study, we investigate the interaction of the cocaine-binding aptamer with quinine. Aptamer variants used in previous studies have been employed here to demonstrate that quinine binds approximately 30-fold more tightly than does cocaine. Furthermore, structural studies using NMR methods in conjunction with thermodynamic studies using isothermal titration calorimetry (ITC) have demonstrated that the ligand-induced folding of the short stem 1 constructs of the cocaine-binding aptamer is retained with the binding of quinine. Noting the similarities between cocaine and quinine (Figure 1), we also investigate the extent of electrostatic interactions taking place with ligand binding.

MATERIALS AND METHODS

Materials. Aptamer samples (Figure 1) were obtained from Integrated DNA Technologies (IDT). The DNA samples were dissolved in distilled deionized H_2O (ddH_2O) and then exchanged three times using a 3 kDa molecular weight cutoff concentrator with sterilized 1 M NaCl followed by three exchanges into ddH_2O. Except where noted, all DNA samples were exchanged with buffer A (20 mM tris(hydroxymethyl)-aminomethane (Tris) (pH 7.4), 140 mM NaCl, and 5 mM KCl) three times before use. These sample conditions are those in which the cocaine-binding aptamer was selected.[12,30] The aptamer concentrations were determined by absorbance spectroscopy using the extinction coefficients supplied by the manufacturer. Quinine hemisulfate monohydrate was obtained from Sigma-Aldrich (catalog number 145912 Aldrich). Stock solutions of quinine hemisulfate were prepared by dissolving the appropriate weight of quinine-hemisulfate monohydrate in buffer A.

Isothermal Titration Calorimetry. ITC was performed using a MicroCal VP-ITC instrument. Data were fit to a one-site binding model using Origin 5.0 software. Samples were degassed prior to use with the MicroCal Thermo Vac unit. All experiments were corrected for the heat of dilution of the titrant. Unless otherwise specified, the quinine and aptamer solutions were prepared in buffer A. The binding experiments were performed with aptamer solutions ranging from 15 to 150 μM using quinine concentrations of 0.23–2.25 mM at the indicated temperatures. All titrations were performed with the aptamer in the cell and with the ligand, as the titrant, in the needle. All aptamer samples were heated in a boiling water bath for 3 min and cooled on ice before use in an ITC experiment, to allow the DNA aptamer to anneal. The standard binding experiments consisted of 35 successive 8 μL injections every 300 s; the first injection was 2 μL. The experimental concentration for the MN4 construct was established using a fixed c value[41] of 50, while the experiments for the MN19 construct used c values ranging from 2 to 7.5. A low-c ITC method was adopted for the weak-binding MN16 construct.[42,43] This method used 20 μM MN16, which was titrated with 3.6 mM quinine to 30-fold molar excess. Experiments using the low-c method consisted of 35 injections in which the first injection was 2 μL, followed by 19 injections of 3 μL and finishing with 15 injections of 15 μL. The injections were made every 300 s. The isobaric change in heat capacity (ΔC_p) of

dx.doi.org/10.1021/bi4010039 | Biochemistry 2013, 52, 8652−8662

quinine binding for MN4 and MN19 was determined by measuring the thermodynamics of binding over temperature ranges of 7.5−35 °C in buffer A. The pH of the Tris buffer was not corrected for changes due to temperature effects. For the ITC-based competitive-binding experiments, the initial titration was performed as described above. Following completion of the first titration, the sample was collected, degassed, and loaded back into the cell; the second titration was then performed with the appropriate ligand.

NMR Spectroscopy. NMR experiments on the aptamer samples were performed using a 600 MHz Bruker Avance spectrometer equipped with a $^{1}H-^{13}C-^{15}N$ triple-resonance probe equipped with triple-axis magnetic-field gradients. All NMR spectra were acquired in $H_2O/^{2}H_2O$ (90%/10%) at 5 °C. These sample conditions, with no NaCl added, were chosen to result in spectra with the smallest linewidths. Nuclear Overhauser enhancement spectroscopy (NOESY) spectra[44,45] were obtained using a mixing time (τ_m) of 200 ms. Water suppression was achieved through the use of the WATERGATE sequence.[46] The aptamer concentration for the NMR studies ranged from 0.4 to 2.3 mM. The two-dimensional (2D) NOESY spectra were processed and analyzed using NMRPipe and NMRDraw.[47]

Small-Angle X-ray Scattering. The MN4 and M19 small-angle X-ray scattering (SAXS) samples were prepared as described for the ITC samples. Matching buffer blanks were prepared using dialysis. A series of dilutions (1/2, 1/4, and 1/8) were also prepared for MN4 and MN19 to ensure that interparticle interference or aggregation was not evident in the highest concentrations. Data acquisition was performed for MN4 and MN19 both free and in complex with quinine and cocaine using an Anton Paar SAXSess mc^2 equipped with a copper microsource, line collimation, and a Mythen 1K detector. The temperature was maintained at 20 °C using a temperature-regulated sample stage. Quartz capillaries were used for the data acquisition. The data reduction was carried out using the program SAXSQuant version 3.8 (Anton Paar). The calculation of pairwise density distribution functions (PDDF) (with desmearing) was performed using the program GIFT, version 05.V.2010. The program GIFT2DAMMIN version 1 (Anton Paar) was used to convert the PDDF files into a format appropriate for the program DAMMIF[48], which was then used to calculate 20 ab initio models of each aptamer MN4 and MN19 free and in complex with quinine and cocaine. The program DAMAVER[48] was used to align and average the ab initio models.

RESULTS

Affinity and Thermodynamics of Quinine Binding. We used ITC methods to establish the affinity and thermodynamics of binding by a set of cocaine aptamer variants for the ligand quinine (Figure 1). The constructs studied were chosen to include the most commonly studied versions of the cocaine-binding aptamer used in our lab and that of others.[31,34,35] Figure 2 provides a sample thermogram of MN4 binding quinine acquired using our ITC methods. The affinity and the thermodynamic parameters of quinine binding for these constructs are summarized in Table 1. These data show that the binding affinity for quinine of the aptamer variants used in this study is consistently significantly higher than that for cocaine. The affinity of MN4 for quinine is 30 times that for cocaine, while the MN19 and WC variants show a 38- and 17-fold increased affinity for quinine over cocaine, respectively.

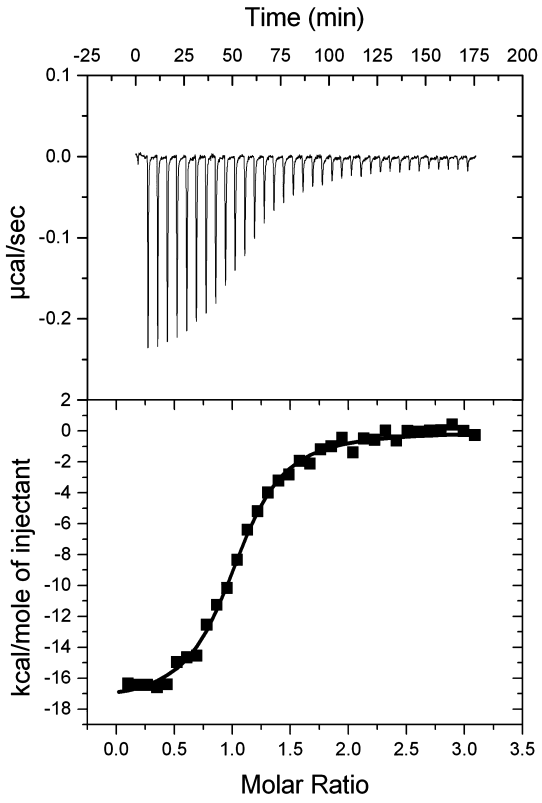

Figure 2. Sample of ITC data showing the interaction of MN4 with quinine. A one-site fit to the data yields a K_d value of 0.16 ± 0.01 μM and an enthalpy of −17.7 kcal mol^{-1}. (Top) The raw titration data showing the heat resulting from each injection of quinine into aptamer solution. (Bottom) The integrated heat plot after correcting for the heat of dilution. This binding experiment was performed at 20 °C in a buffer of 20 mM Tris (pH 7.4), 140 mM NaCl, and 5 mM KCl.

Table 1. Thermodynamic Parameters for the Interaction between Quinine and the Aptamers Presented in This Study[a]

	quinine			cocaine[b]
aptamer	K_d (μM)	ΔH (kcal mol^{-1})	$-T\Delta S$ (kcal mol^{-1})[a]	K_d (μM)
MN4	0.23 ± 0.03	−14.5 ± 0.4	5.6 ± 0.4	7 ± 1
MN19	0.7 ± 0.2	−22.2 ± 0.4	14.0 ± 0.4	26.7 ± 0.7
WC	12 ± 4	−21 ± 4	15 ± 4	204 ± 6
MN16	51 ± 3	−6.9 ± 0.5	1.1 ± 0.4	vwb[c]
MN4 + Mg^{2+}	0.42 ± 0.02	−10.9 ± 0.7	2.4 ± 0.7	nd[c]
MN19 + Mg^{2+}	0.6 ± 0.4	−14.6 ± 1.6	6.4 ± 1.4	nd

[a]Data acquired in a buffer of 20 mM Tris (pH 7.4), 140 mM NaCl, and 5 mM KCl. Data for WC, MN4, and MN16 were acquired at 20 °C; data for MN19 were acquired at 17.5 °C; data for MN4 and MN19 with Mg^{2+} were acquired at 15 °C. The values reported are averages of 2−5 individual experiments. The error range reported is one standard deviation. [b]The corresponding data for cocaine binding are included for the purpose of comparison.[35] [c]vwb denotes that only very weak binding was observed; nd denotes not determined, the experiment was not performed.

These data also demonstrate that the relative order of affinity for these aptamers remains the same for both the quinine and the cocaine ligands. Among the variants studied, the MN4 exhibits the highest affinity. The ITC data further demonstrate

dx.doi.org/10.1021/bi4010039 | Biochemistry 2013, 52, 8652−8662

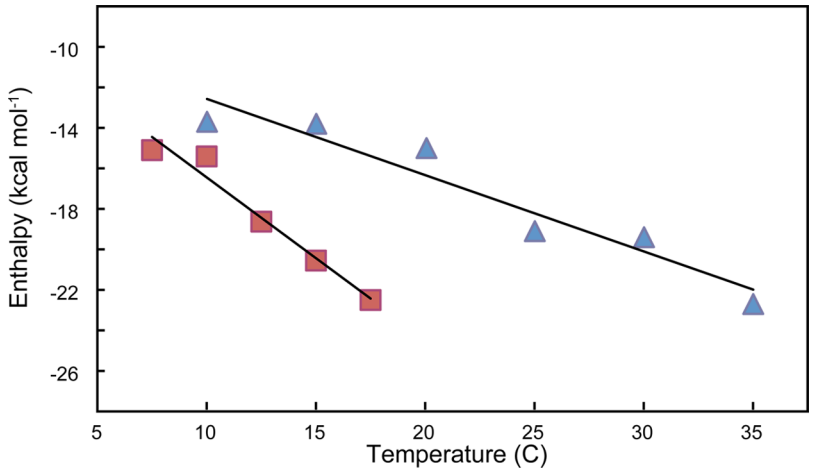

Figure 3. Temperature dependence of the enthalpy of MN4 (triangles) and MN19 (squares) binding quinine. The slope of the line represents ΔC_p, which was determined to be -377 ± 55 cal mol^{-1} K^{-1} for MN4 and -798 ± 91 cal mol^{-1} K^{-1} for MN19. The more negative ΔC_p for MN19 implies a larger extent of folding with ligand binding. Binding experiments were performed in a solution of 20 mM Tris (pH 7.4), 140 mM NaCl, and 5 mM KCl.

that, for all aptamer variants used in this study, quinine binding is an enthalpically driven process with unfavorable binding entropy.

Previous studies have indicated that DNA structures containing three-way junctions are more stable in the presence of Mg^{2+}.[49] To see if the presence of Mg^{2+} affects quinine binding, we performed ITC experiments using MN4 and MN19 in the presence of buffer A that also contains 5 mM $MgCl_2$. The results of these experiments are in Table 1 and show that the addition of $MgCl_2$ has a negligible effect on the affinity of these aptamers for quinine.

Change in Heat Capacity with Quinine Binding. To gain a greater level of insight into the mechanism by which the MN4 and MN19 aptamers bind quinine, we measured the enthalpy of binding by these aptamers as a function of temperature to determine the change in heat capacity of binding (ΔC_p). These data are plotted in Figure 3. For MN4, temperature data were obtained from 10 to 35 °C. Binding data for MN19 was acquired from 7.5 to 17.5 °C. At temperatures above 17.5 °C, MN19 exhibited signs of incomplete folding upon binding as the enthalpy rapidly became less negative, and it is not possible to separate the enthalpy of folding from that of binding. From the slopes of the lines in Figure 3, we compute that the value of ΔC_p for MN4 is -377 ± 55 cal mol^{-1} K^{-1} and that the value of ΔC_p for MN19 is -798 ± 91 cal mol^{-1} K^{-1}.

Buffer Identity and Quinine Binding. We used ITC methods to test for changes in the protonation state of quinine during binding. Change in protonation is detected by measuring the binding enthalpy in different buffers at a constant pH value. If the protonation state changes during binding, different binding enthalpy values will be obtained that differ by the number of protons lost or gained, multiplied by the protonation enthalpy of the buffer.[50,51] We measured the enthalpies of MN4 binding to quinine in both *N*-(2-hydroxyethyl)piperazine-N′-ethanesulfonic acid (HEPES) and phosphate buffer at a pH value of 7.4 to be -15.2 ± 0.8 kcal mol^{-1} and -14.4 ± 1.4 kcal mol^{-1}, respectively. We also measured binding at pH 8.5 using Hepes and Tris buffer and obtained ΔH values of -14.2 ± 0.5 kcal mol^{-1} and -16.7 ± 1.6 kcal mol^{-1}, respectively. The similarity of the binding enthalpies in the two buffers at each of these pH values indicates that little to no change in protonation state is taking place with quinine binding. If the protonation state changed, the expected difference in ΔH values would be 16 and 11 kcal mol^{-1}, respectively.

Effect of Ionic Strength on Quinine Binding. To quantify the contribution that electrostatic interactions play in quinine binding, we determined the enthalpy of MN4 binding quinine at a range of NaCl concentrations from 50 to 500 mM. In general, the affinity of the aptamer for quinine increases as the NaCl concentration decreases. The contribution of electrostatics to ligand binding is measured by eq 1, where Z is the apparent charge on the bound ligand and φ is the fraction of Na^+ bound per nucleic acid phosphate.[52]

$$\left(\frac{\partial \log K_a}{\partial \log[Na^+]}\right) = -Z\varphi \quad (1)$$

From a plot of log K_a versus log [NaCl] the slope gives the value of $-Z\varphi$. For MN4 binding quinine (Figure 4) this value is -0.45 ± 0.14. The contribution of electrostatics to the free energy of binding can then be determined from eq 2.

$$\Delta G_{elec} = Z\varphi RT \ln[Na^+] \quad (2)$$

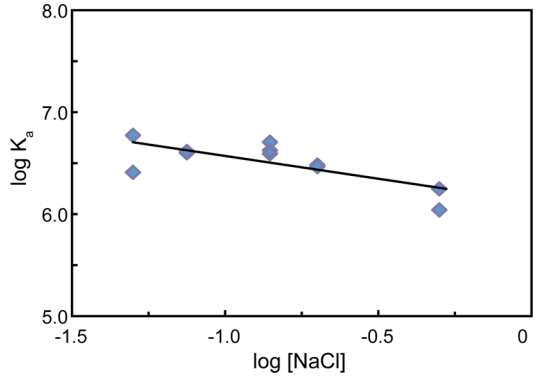

Figure 4. Log K_a vs log [NaCl] for MN4 binding to quinine. The slope of this line was used to determine the contribution to the free energy of binding by electrostatic (ΔG_{elec}) interactions. At 140 mM NaCl, ΔG_{elec} comprises only 6% of the overall binding ΔG.

dx.doi.org/10.1021/bi4010039 | *Biochemistry* 2013, 52, 8652−8662

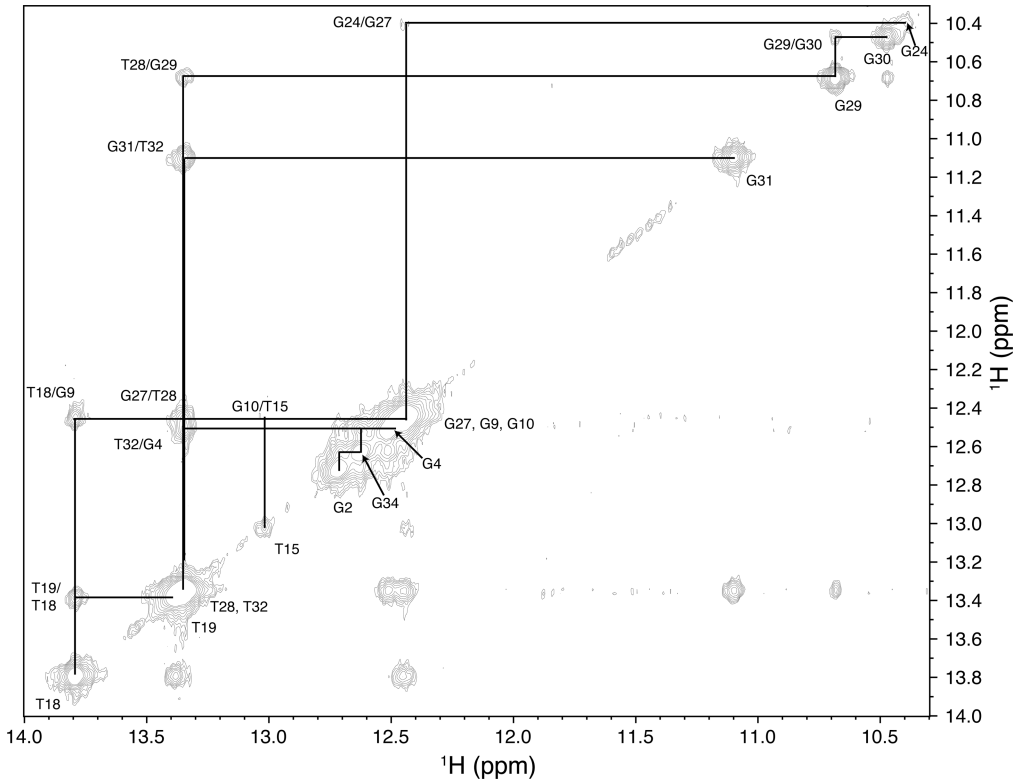

Figure 5. Imino−imino region of the 2D NOESY spectrum (τ_m = 200 ms) of MN4 bound to quinine acquired in 10% D_2O/90% H_2O at 5 °C. Assignments are traced out in the spectrum.

For the MN4−quinine pair the value of ΔG_{elec} is −0.51 kcal mol^{-1} at 140 mM NaCl. Knowing the binding affinity at this NaCl concentration (Table 1) we determine that the overall binding free energy is −8.90 kcal mol^{-1}. This shows that the contributions of electrostatics represent 6% of the overall free energy of MN4 binding quinine at 140 mM NaCl.

NMR Assignments and Quinine-Induced Chemical Shift Perturbations. The ^{1}H NMR assignment of the imino protons of the quinine-bound MN4 and MN19 aptamers were obtained from 2D homonuclear NOESY experiments. The quality of the NMR data was excellent, and complete assignments of the imino protons were obtained for the spectra of both quinine-bound MN4 and quinine-bound MN19 (Figures 5, 6, Supporting Information Figure 1). For MN19, in which stem 1 contains three base pairs, the aptamer is not fully folded in the free state.[35] This is shown in Figure 6b, in which MN19 in the free state displays only four imino proton signals. Upon addition of quinine, new signals appear from the bound MN19, and we observe all the expected peaks in the equimolar sample of MN19 with quinine.

Insights into the location of the quinine-binding site in the MN4 aptamer can be deduced from the chemical-shift perturbations of the imino protons observed with ligand binding. Assignments of free MN4 were known from a previous study[31] and match what was observed for this sample of free MN4. The binding of quinine is in slow exchange on the NMR time scale, with signals for both the free and bound resonances observed simultaneously upon addition of quinine. We can determine the difference in chemical shift between the free and quinine-bound states, plotted in Figure 7. Upon binding, G31 showed the greatest shift of imino resonance, followed by T32 and T28. As seen previously with MN4, we do not observe the imino resonance of T19 in the free sample, but that resonance appears with ligand binding (Figures 5 and 6).

ITC and NMR-Monitored Competition Binding Experiments. To determine if the cocaine and quinine ligands bind at the same location in the aptamer, we performed a set of ITC-monitored competitive-binding experiments (Figure 8). First, we added quinine to a solution of free MN4 (Figure 8a). From fitting the data to a single-site binding model, we obtained a K_d value of 0.35 ± 0.04 μM and a ΔH value of −15.2 ± 0.2 kcal mol^{-1} at 15 °C. Following this experiment, we titrated cocaine into a solution of the quinine-bound MN4. As seen in Figure 8b no detectable binding was observed. This inability of cocaine to bind MN4 in the presence of quinine is consistent with quinine being bound tighter by MN4 and with both ligands binding at the same site in the aptamer. Additionally, we performed the reverse experiment in which cocaine was first added to MN4 (Figure 8c), resulting in a K_d value of 2.2 ± 0.1 μM and a ΔH value of −7.96 ± 0.08 kcal mol^{-1} at 15 °C. Next, we titrated quinine into the cocaine-bound MN4 and observed binding (Figure 8d). We fit these titration data to a competitive-binding model[53], which resulted in a K_d value of 0.14 ± 0.02 μM and a ΔH value of −11.2 ± 0.1 kcal mol^{-1} at 15 °C for quinine binding to MN4.

Competitive binding by cocaine and quinine for MN4 was also observed in NMR-monitored titrations. Three different titrations were performed. First, quinine was added to MN4 followed by addition of cocaine (Supporting Information, Figure 2). During the addition of quinine, similar changes were observed, as seen in Figure 6a. During the addition of cocaine to the quinine-bound MN4, no changes in chemical shift were observed; however, peaks due to G31, T15, and T18 experienced significant line broadening. In the second NMR-monitored titration, cocaine was first added to MN4, followed

dx.doi.org/10.1021/bi4010039 | Biochemistry 2013, 52, 8652−8662

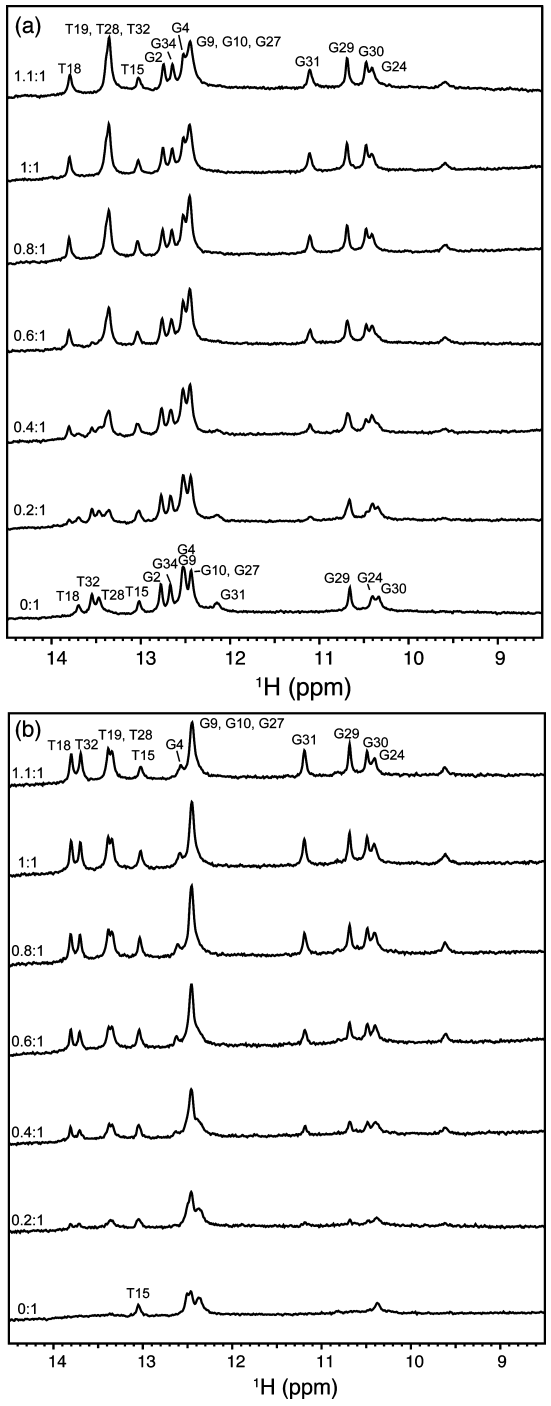

Figure 6. Quinine binding monitored by one-dimensional (1D) ^{1}H NMR. Displayed is the region of the NMR spectrum focusing on the imino resonances as a function of increasing quinine concentration. (a) Spectra of MN4 titrated with quinine. (b) Spectra of MN19 titrated with quinine. Note that for MN19 only a few broad peaks are observed in the free spectrum. Upon binding, sharp resonances from the quinine-bound MN19 aptamer appear. All spectra were acquired in 90% H_2O/10% ^2H_2O at 5 °C at the molar ratio of quinine to aptamer indicated.

by the addition of quinine to the MN4-cocaine complex (Supporting Information, Figure 3). The first part of this titration resulted in spectra that are very similar to those we observed previously for the addition of cocaine to MN4.[31] When quinine was added to the MN4−cocaine complex, we

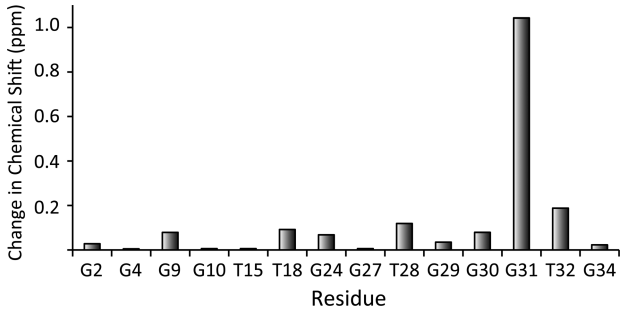

Figure 7. Histogram showing the chemical shift perturbations of the imino protons in MN4 upon quinine binding.

did observe some peaks change their chemical shift. Namely, the peak due to G31 shifted to its frequency indicative of the quinine-bound MN4, and the peak due to T19 shifted to its quinine-bound frequency. Additionally, in the spectrum acquired with a molar ratio of 1:1.1:3 (MN4/cocaine/quinine) all the peaks experience line broadening and resonances from T18, and T15 experienced line broadening to an extent such that peaks are not observed. Finally, we performed a titration where an equimolar mixture of cocaine and quinine was added to MN4 (Supporting Information, Figure 4). In this titration, at subsaturating amounts of total ligand concentration, we observe peaks from both quinine-bound G31 and cocaine-bound G31 simultaneously. These peaks are best observed at a molar ratio of 1:0.375:0.375 (MN4/cocaine/quinine). As the total ligand concentration increases, the proportion of MN4 bound to the more tightly binding quinine increases, and the amount of cocaine-bound MN4 decreases. Note that all three titrations include a spectrum in which the molar ratios of MN4 and the two ligands are essentially the same. This is the 1:1:1 (MN4/cocaine/quinine) spectrum that corresponds to MN4 87.4% quinine-bound and 12.4% cocaine-bound. The MN4 spectrum at this ratio appears very similar in all three titrations, demonstrating the repeatability of these titrations despite the different titration schemes used.

SAXS Structural Analysis. SAXS studies were pursued to further characterize the solution structure of the MN4 and MN19 aptamers. Scattering data for the unbound samples of both aptamers as well as each aptamer bound to cocaine and quinine are shown in Figure 9A. Also shown in Figure 9A are the desmeared scattering curves that were used for subsequent analysis. PDDF plots for each sample are shown in Figure 9B, and SAXS structural parameters are reported in Table 2. The radius of gyration (R_g) was determined by Guinier analysis and from the PDDF plots. Both methods produced consistent R_g estimates. The R_g was consistently larger for the MN4 aptamer than it was for the MN19 aptamer, for both free and bound forms, ranging from 17.5 to 17.8 Å and from 15.5 to 15.8 Å for MN4 and MN19, respectively. Similarly the R_{max} is larger for MN4 than it is for MN19, ranging from 57 to 58 Å and from 45 to 47 Å, respectively. The PDDFs indicate that the MN4 free and the quinine- and cocaine-bound samples exhibit similar solution structures, while the MN19 samples are quite different (Figure 9B). This is particularly evident when comparing the free MN19 data with that of the two bound aptamer samples. The MN4 PDDFs exhibit a bimodal pattern that is most likely due to the defined distances between at least two of the stem loops of the aptamer. A less obvious bimodal pattern is present in the MN19 PDDF plots. A shoulder is evident in the free

dx.doi.org/10.1021/bi4010039 | *Biochemistry* 2013, 52, 8652−8662

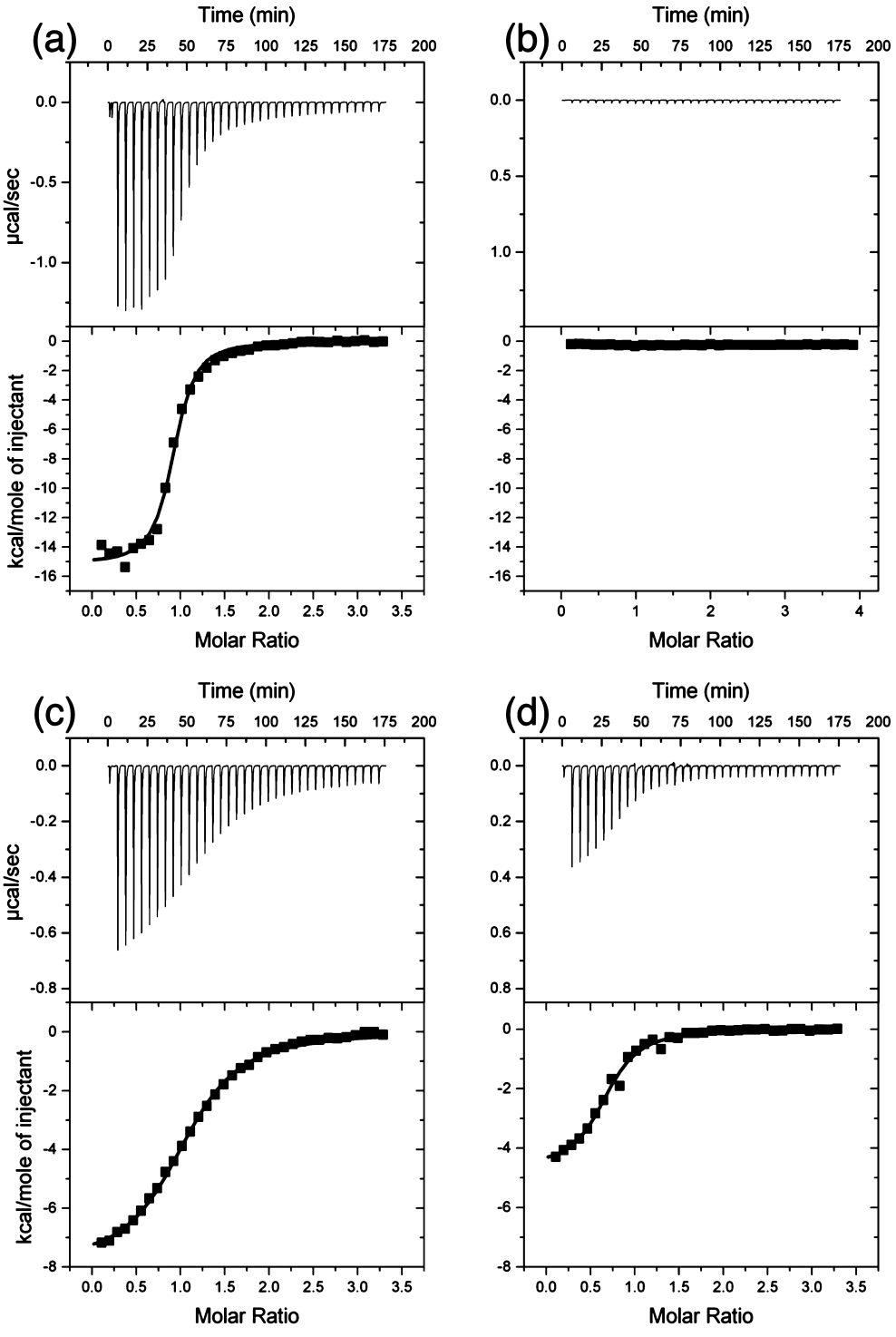

Figure 8. ITC-based competitive-binding data. Shown are the interactions of (a) quinine with unbound MN4, (b) cocaine with quinine-bound MN4, (c) cocaine with unbound MN4, and (d) quinine into cocaine-bound MN4. On the top of each panel is the raw titration data showing the heat resulting from each injection of quinine into aptamer solution. On the bottom of each panel is the integrated heat plot after correcting for the heat of dilution. Titrations (a) and (c) were fit to a single-site binding model, while the titration in (d) was fit to a competitive-binding model. All binding experiments were performed at 15 °C in a buffer of 20 mM Tris (pH 7.4), 140 mM NaCl, and 5 mM KCl.

MN19 PPDF plot at approximately 35 Å and in the bound MN19 PDDF plots at 28 Å on the *r* axis.

The ab initio shape reconstructions for MN4 and MN19 free and in complex with either quinine or cocaine are shown in Figure 9C,D, respectively. The normalized spatial discrepancy (NSD) for each sample indicates that reconstructions provide meaningful results (Table 2). Examination of the reconstructions of the MN4 aptamer shows the similarity of the structures, both in absence and in presence of ligand. Conversely, aptamer MN19 exhibits differences between the free aptamer and the quinine and cocaine complexes. The MN4 aptamer and complexes are elongated with a significant bulge on one side, while the MN19 aptamer and complexes exhibit a range of different shapes (Figure 9C,D).

dx.doi.org/10.1021/bi4010039 | *Biochemistry* 2013, 52, 8652−8662

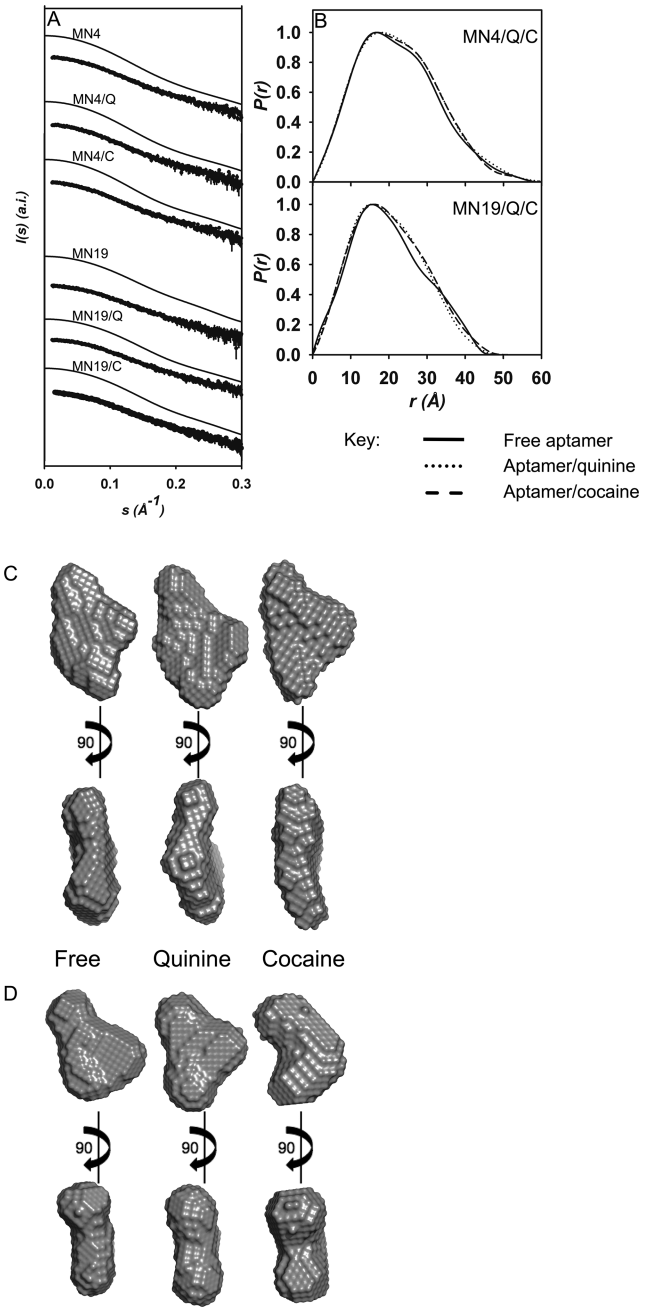

Figure 9. SAXS analysis of MN4 and MN19 free and bound to quinine or cocaine. (A) Scattering data for each sample showing raw scattering data with error bars; above this, the desmeared scattering curve. (B) PDDF plots. Top panel MN4; MN4/Q and MN4/C indicate MN4 bound to quinine and cocaine, respectively. Bottom panel MN19; MN19/Q and MN19/C indicate MN19 bound to quinine and cocaine, respectively. (C) Ab initio reconstructions of free MN4 and MN4 with quinine or cocaine bound. (D) Ab initio reconstructions of free MN19 and MN19 with quinine or cocaine bound. Two orientations rotated 90° about the *y* axis are presented. The reconstructions were aligned using the program supcomb.[57]

DISCUSSION

In this study we analyze the binding of quinine by the cocaine-binding aptamer. This work provides a basis for comparing the binding thermodynamics of the aptamers MN4 and MN19 for cocaine, the ligand originally used to select these aptamers, and what we present here for quinine. We find that there are many similarities in the binding mechanism between these two ligands and also some differences. From the competition binding experiments (Figure 8), we show that the cocaine and quinine share a common binding site in the aptamer as opposed to binding at separate sites. Perhaps most significantly we find that the MN4 and MN19 aptamers bind quinine 30−40 times more tightly than they bind cocaine (Table 1). It is unusual for an aptamer to bind an off-target ligand much more tightly than the ligand it has been selected for. Quinine and cocaine do share some common structural features in that they both have an aromatic ring attached to an aliphatic nitrogen-containing eight-atom bridged ring structure (Figure 1). However, these two structures are significantly different in the location of the substituents on the aliphatic ring. When the aliphatic ring portions of the molecule are superimposed to align the nitrogen atoms, there is little overlap of the aromatic rings. Similarly, overlaying the aromatic rings results in the aliphatic portion of the molecule not being aligned to any significant extent. However, it is possible that in the binding site, bonds in the ligands rotate into conformations other than those most favored in the free state. Detailed structural analysis of the complexes formed between the ligands and the aptamer are needed to understand how the cocaine binding aptamer interacts with both cocaine and quinine.

Table 2. Structural Parameters Calculated from SAXS Data

sample	R_g (Å)[a]	R_g (Å)[b]	R_{max} (Å)	NSD[c]
MN4	17.5	17.6	57	0.83
MN4/quinine	17.8	17.8	57	0.72
MN4/cocaine	17.6	17.5	58	0.76
MN19	15.7	15.7	45	0.64
MN19/quinine	15.5	15.4	46	0.56
MN19/cocaine	15.8	15.8	47	0.55

[a]R_g calculated from Guinier plot of desmeared scattering data. [b]R_g calculated from PDDF. [c]Normalized spatial discrepancy.

The exact reason for our observed increased affinity for quinine over cocaine is still unknown, but this affinity may be due more to the presence of the larger bicyclic aromatic ring on quinine than to the smaller monocyclic aromatic ring found in cocaine (Figure 1). The larger aromatic group in quinine may provide an increase in stacking interactions with the DNA bases in the aptamer compared to those seen in cocaine. In support of stacking interactions playing a role in the cocaine binding aptamer−ligand interactions, we note that the combination of binding enthalpy and entropy for both quinine and cocaine by this aptamer (Table 1) falls into the intercalator category by the classification of Chaires.[54]

Additional support of the importance of the aromatic ring in ligand binding by the cocaine binding aptamer is found when comparing the binding of quinine and cocaine to that of their structural analogues. The quinine analogues cinchonine and cinchonidine are identical to quinine except they are missing the methoxy group present in quinine on the aromatic ring (Figure 11). Both of these ligands are bound significantly more weakly than quinine by the cocaine-binding aptamer despite this minor change.[38,40] In comparison, data consistent with changes to the aliphatic portion of the ligand not being important for binding come from studies by the Heemstra group in which both cocaine and norcocaine (Figure 11) have equal effect in their split aptamer proximity ligation assay.[36,37] In contrast, removal of the aromatic group from cocaine (ecgonine methyl ester) and the creation of a negatively

dx.doi.org/10.1021/bi4010039 | Biochemistry 2013, 52, 8652−8662

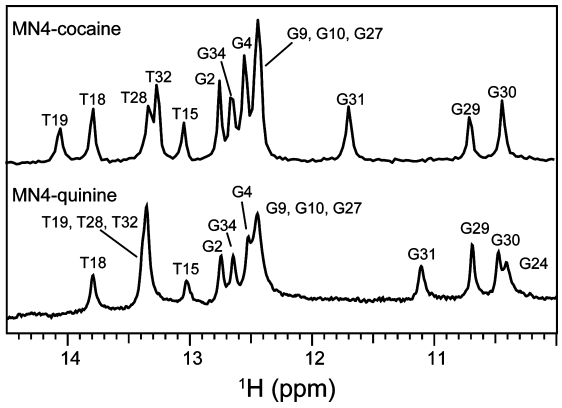

Figure 10. Comparison of the imino region of the 1D ^{1}H NMR spectra of cocaine- and quinine-bound MN4 aptamer. For most imino protons, their resonances occur at the same position in both spectra, indicating the similarity of the structure for both aptamers. The only significant differences between these two spectra are the positions of the G31 and T19 imino protons. These protons lie at the binding site, and the change in frequency of these imino resonances in the two samples reflects the different bound ligand.

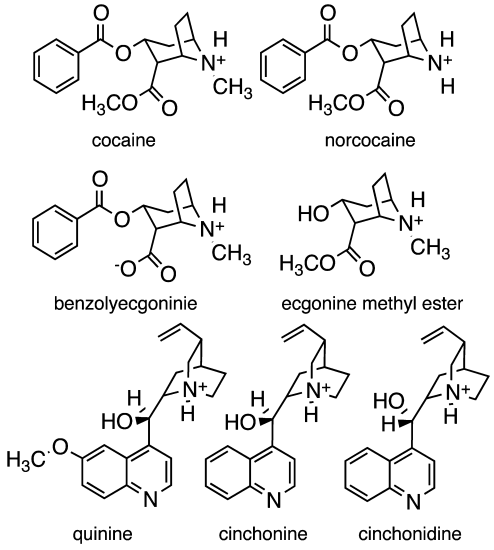

Figure 11. Chemical structures of quinine, cocaine, and a series of structural analogues.

charged carboxylic acid by the removal of a methyl group on cocaine to make benzoylecgonine both result in very little ligation due to these ligands not being bound by the cocaine-binding aptamer.[36,37] Together, these data indicate that changes to the aromatic portion of the ligand result in a significant decrease in binding affinity.

The functionally important structural-switching binding mechanism for the short stem 1 aptamer construct, MN19, is retained for both the cocaine and the quinine ligands. When stem 1 is shortened to three base pairs, few imino signals are seen in the 1D ^{1}H NMR (Figure 6), indicating the aptamer has a limited number of base pairs stably formed in the unbound state. Upon addition of quinine, all the expected imino signals for the secondary structure shown in Figure 1 appear. For MN4, the aptamer is folded in the free state, and quinine binding, like cocaine binding, does not appear to significantly change the secondary structure of the aptamer. Additional evidence for the structure switching mechanism is displayed by the ΔC_p data for MN4 and MN19. We observe a more negative ΔC_p for MN19 binding quinine than we do for MN4 binding quinine (Figure 3). The basis for a negative ΔC_p is the burying of nonpolar surface area.[55] This can result directly from burying the ligand as well as indirectly by triggering folding in the aptamer, resulting in an increase in nonpolar surface being buried as base stacking increases. In our case, we expect quinine binding by both MN19 and MN4 to result in a similar amount of nonpolar surface area burial on the ligand, and we expect any difference between the MN4 and MN19 aptamers to reflect differences in nonpolar burial due to folding. For MN19, if the aptamer starts off more unfolded in the free state than the bound state, and aptamer folding occurs with quinine binding, a more negative ΔC_p is expected than if the aptamer is folded in both the free and bound state. Demonstrated here, quinine binding to MN19 has a ΔC_p of -798 ± 91 cal mol^{-1} K^{-1}, while the ΔC_p for MN4 is -377 ± 55 cal mol^{-1} K^{-1}. This more negative ΔC_p for MN19 is consistent with a ligand-induced folding mechanism. Similarly, we saw a more negative ΔC_p with the short stem 1 construct, MN6, binding cocaine compared to MN4 binding cocaine.[31] Additionally, we observed this trend for the binding of deoxycholic acid by the short stem 1 construct MS2 has a more negative ΔC_p value than the long stem 1 construct.[34] This structural-switching binding mechanism is likely inherent in this aptamer and can be triggered by binding any ligand that provides enough binding free energy to trigger folding.

Evidence for a difference between the MN4 and MN19 binding mechanism is supported by the SAXS data presented in this study. For MN4, the PDDF plot (Figure 9B) shows little difference between the free MN4 form and the two ligand-bound complexes, indicating that only small structural changes, if any, occur upon ligand binding. In contrast, for MN19 the PDDF plot shows significant differences between the three forms of the aptamer. The free MN19 aptamer exhibits a shoulder around 35 Å not seen in the quinine- and cocaine-bound forms of the aptamer. The ab initio shape reconstruction of the MN4 and MN19 aptamers shows this molecule forms a nonglobular, elongated, and flat structure (Figure 9C,D). The three MN4 structures are fairly similar, containing a bulge off to one side, while the three MN19 structures form variations of an elongated flat structure.

From the NMR chemical shift perturbation data, we conclude that quinine and cocaine share a common ligand-binding site. The signals that move most with quinine binding are G31 and T32 (Figures 6, 7, and 9). These are the same resonances that move the most with cocaine binding.[31] Additionally, the T19 imino signal appears in the quinine-bound sample, while it is not observable in the free MN4 state. The main difference in the imino-proton NMR spectrum of the cocaine- and quinine-bound aptamer is that G31 has a greater change in chemical shift with quinine binding than it does when binding cocaine. Also, the position of the bound T19 is significantly different in these two forms (Figure 10). Changes in chemical shifts can be due to the spatial proximity of the ligand and the observed proton or to structural changes with ligand binding at a site away from the location of the observed proton resonance. We think that in this case, the perturbation is due to direct contact: if ligand binding was occurring at a site away from the site of the greatest change in chemical shift, signals other than G31, T32, and T19 would be affected by the binding event. Together this implies not only that the ligand-binding location in the aptamer is the same for both cocaine

dx.doi.org/10.1021/bi4010039 | Biochemistry 2013, 52, 8652−8662

and quinine but also that the binding site is close to T32, G31, and T19.

The salt-dependent behavior of the quinine-binding association constant shows that the MN4 aptamer uses electrostatics for only about 6% of the binding free energy at a NaCl concentration of 140 mM. This is small compared with the binding of aminoglycosides to the A-site RNA, in which electrostatics make up >50% of the binding free energy.[56] This difference reflects the number of charged amino groups involved in the interaction between the ligand and nucleic acid binding partners, but it also likely reflects the need for aptamers to use more shape-specific interactions, such as hydrogen bonds, to specifically recognize their desired ligand, even though this aptamer distinguishes poorly between cocaine and quinine.

In summary, we demonstrate that quinine binding by the cocaine-binding aptamer is similar to the enthalpy-driven binding mechanism the aptamer has for cocaine, follows a ligand-induced folding similar to that for cocaine when stem 1 is three base pairs long, and shares with cocaine the same ligand-binding site in the aptamer. The major difference between the two ligands is the significantly higher affinity of the aptamer for quinine over cocaine. While the lack of ligand-binding specificity of the cocaine-binding aptamer raises doubts about the suitability of this aptamer for biosensor applications, it does allow the nonbiosensor uses of this aptamer to be developed using quinine as opposed to cocaine.

■ ASSOCIATED CONTENT

Supporting Information

Figure of (1) 2D NOESY showing the assignment of MN19 bound to quinine; (2) 1D ^{1}H NMR of a titration of quinine into MN4 followed by a titration of cocaine into the MN4/quinine complex; (3) 1D ^{1}H NMR of a titration of cocaine into MN4 followed by a titration of quinine into the MN4/cocaine complex; and (4) 1D ^{1}H NMR of a titration of a 1:1 mixture of cocaine and quinine into MN4. This material is available free of charge via the Internet at http://pubs.acs.org.

■ AUTHOR INFORMATION

Corresponding Author

*E-mail: pjohnson@yorku.ca. Tel.: 416-736-2100 x3319. Fax: 416-736-5936.

Funding

This work was supported by funding from York University and the Natural Sciences and Engineering Research Council of Canada (NSERC) to P.E.J.; M.C.J.W. is funded by both the Australian Research Council and the National Health and Medical Research Council of Australia.

Notes

The authors declare no competing financial interest.

■ ACKNOWLEDGMENTS

We thank Ella Galpern for drawing the graphical abstract, Sina Haftchenary (University of Toronto) for help with providing a copy of Origin7, Anne Johnson (Ryerson University, Toronto) for useful discussion about competitive binding, and members of the Johnson lab (York University, Toronto) and Wilce lab (Monash University, Clayton, Australia) for additional useful discussions.

■ ABBREVIATIONS

ΔC_p, change in heat capacity at constant pressure; ITC, isothermal titration calorimetry; K_d, dissociation constant; NMR, nuclear magnetic resonance; R_g, radius of gyration; SAXS, small-angle X-ray scattering

■ REFERENCES

(1) Liu, J., Cao, Z., and Lu, Y. (2009) Functional Nucleic Acid Sensors. *Chem. Rev. 109*, 1948−1998.

(2) Li, D., Song, S., and Fan, C. (2010) Target-Responsive Structural Switching for Nucleic Acid-Based Sensors. *Acc. Chem. Res. 43*, 631−641.

(3) Cho, E. J., Lee, J.-W., and Ellington, A. D. (2009) Applications of Aptamers As Sensors. *Annu. Rev. Anal. Chem. 2*, 241−264.

(4) Xing, H., Wong, N. Y., Xiang, Y., and Lu, Y. (2012) DNA Aptamer Functionalized Nanomaterials for Intracellular Analysis, Cancer Cell Imaging and Drug Delivery. *Curr. Opin. Chem. Biol. 16*, 429−435.

(5) Du, Y., Li, B., and Wang, E. (2012) "Fitting" Makes "Sensing" Simple: Label-Free Detection Strategies Based on Nucleic Acid Aptamers. *Acc. Chem. Res. 46*, 203−213.

(6) Iliuk, A. B., Hu, L., and Tao, W. A. (2011) Aptamer in Bioanalytical Applications. *Anal. Chem. 83*, 4440−4452.

(7) Famulok, M., and Mayer, G. (2011) Aptamer Modules As Sensors and Detectors. *Acc. Chem. Res. 44*, 1349−1358.

(8) Vallee-Belisle, A., and Plaxco, K. W. (2010) Structure-Switching Biosensors: Inspired by Nature. *Curr. Opin. Struct. Biol. 20*, 518−526.

(9) Ellington, A. D., and Szostak, J. W. (1990) In vitro Selection of RNA Molecules That Bind Specific Ligands. *Nature 346*, 818−822.

(10) Tuerk, C., and Gold, L. (1990) Systematic Evolution of Ligands by Exponential Enrichment: RNA Ligands to Bacteriophage T4 DNA Polymerasae. *Science 249*, 505−510.

(11) Stojanovic, M. N., and Worgall, T. S. (2010) Detecting Hydrophobic Molecules with Nucleic Acid-Based Receptors. *Curr. Opin. Chem. Biol. 14*, 751−757.

(12) Stojanovic, M. N., de Prada, P., and Landry, D. W. (2001) Aptamer-Based Folding Fluorescent Sensor for Cocaine. *J. Am. Chem. Soc. 123*, 4928−4931.

(13) Stojanovic, M. N., and Landry, D. W. (2002) Aptamer-Based Colorimetric Probe for Cocaine. *J. Am. Chem. Soc. 124*, 9678−9679.

(14) Zhang, J., Wang, L., Pan, D., Song, S., Boey, F. Y. C., Zhang, H., and Fan, C. (2008) Visual Cocaine Detection with Gold Nanoparticles and Rationally Engineered Aptamer Structures. *Small 4*, 1196−1200.

(15) Madru, B., Chapuis-Hugon, F., Peyrin, E., and Pichon, V. (2009) Determination of Cocaine in Human Plasma by Selective Solid-Phase Extraction Using an Aptamer-Based Sorbent. *Anal. Chem. 81*, 7081−7086.

(16) Baker, B. R., Lai, R. Y., Wood, M. S., Doctor, E. H., Heeger, A. J., and Plaxco, K. W. (2006) An Electronic, Aptamer-Based Small-Molecule Sensor for the Rapid, Label-Free Detection of Cocaine in Adulterated Samples and Biological Fluids. *J. Am. Chem. Soc. 128*, 3138−3139.

(17) Liu, J., Mazumdar, D., and Lu, Y. (2006) A Simple and Sensitive "Dipstick" Test in Serum Based on Lateral Flow Separation of Aptamer-Linked Nanostructures. *Angew. Chem., Int. Ed. 45*, 7955−7959.

(18) Li, T., Li, B., and Dong, S. (2007) Adaptive Recognition of Small Molecules by Nucleic Acid Aptamers through a Label-Free Approach. *Chem.—Eur. J. 13*, 6718−6723.

(19) Chen, J., Jiang, J., Gao, X., Liu, G., Shen, G., and Yu, G. (2008) A New Aptameric Biosensor for Cocaine Based on Surace-Enhanced Raman Scattering Spectroscopy. *Chem.—Eur. J. 14*, 8374−8382.

(20) Swensen, J. S., Xiao, Y., Ferguson, B. S., Lubin, A. A., Lai, R. Y., Heeger, A. J., Plaxco, K. W., and Soh, H. T. (2009) Continuous, Real-Time Monitoring of Cocaine in Undiluted Blood Serum via a Microfluidic, Electrochemical Aptamer-Based Sensor. *J. Am. Chem. Soc. 131*, 4262−4266.

(21) Xiang, Y., and Lu, Y. (2011) Using Personal Glucose Meters and Functional DNA Sensors to Quantify a Variety of Analytical Targets. *Nat. Chem. 3*, 697−703.
(22) Yang, K.-A., Pei, R., Stefanovic, D., and Stojanovic, M. N. (2011) Optimizing Cross-Reactivity with Evolutionary Search for Sensors. *J. Am. Chem. Soc. 134*, 1642−1647.
(23) Porchetta, A., Vallee-Belisle, A., Plaxco, K. W., and Ricci, F. (2012) Using Distal Site Mutations and Allosteric Inhibition to Tune, Extend, and Narrow the Useful Dynamic Range of Aptamer-Based Sensors. *J. Am. Chem. Soc. 134*, 20601−20604.
(24) Das, J., Cederquist, K. B., Zaragoza, A. A., Lee, P. E., Sargent, E. H., and Kelley, S. O. (2012) An Ultrasensitive Universal Detector Based on Neutralizer Displacement. *Nat. Chem. 4*, 642−648.
(25) Zhou, J., Ellis, A. V., Kobus, H., and Voelcker, N. H. (2012) Aptamer Sensor for Cocaine Using Minor Groove Binder Based Energy Transfer. *Anal. Chim. Acta 719*, 76−81.
(26) Zou, R., Lou, X., Ou, H., Zhang, Y., Wang, W., Yuan, M., Guan, M., Luo, Z., and Liu, Y. (2012) Highly Specific Triple-Fragment Aptamer for Optical Detection of Cocaine. *RSC Adv. 2*, 4636−4638.
(27) Freeman, R., Sharon, E., Tel-Vered, R., and Willner, I. (2009) Supramolecular Cocaine−Aptamer Complexes Activate Biocatalytic Cascades. *J. Am. Chem. Soc. 131*, 5028−5029.
(28) Wang, Z.-G., Wilner, O. I., and Willner, I. (2009) Self-Assembly of Aptamer−Circular DNA Nanostructures for Controlled Biocatalysis. *Nano Lett. 9*, 4098−4102.
(29) Freeman, R., Sharon, E., Teller, C., and Willner, I. (2010) Control of Biocatalytic Transformations by Programmed DNA Assemblies. *Chem.—Eur. J. 16*, 3690−3698.
(30) Stojanovic, M. N., de Prada, P., and Landry, D. W. (2000) Fluorescent Sensors Based on Aptamer Self-Assembly. *J. Am. Chem. Soc. 122*, 11547−11548.
(31) Neves, M. A. D., Reinstein, O., and Johnson, P. E. (2010) Defining a Stem Length-Dependant Binding Mechanism for the Cocaine-Binding Aptamer. A Combined NMR and Calorimetry Study. *Biochemistry 49*, 8478−8487.
(32) Cekan, P., Jonsson, E. O., and Sigurdsson, S. T. (2009) Folding of the Cocaine Aptamer Studied by EPR and Fluorescence Spectroscopies Using the Bifunctional Spectroscopic Probe Ç. *Nucleic Acids Res. 37*, 3990−3995.
(33) Stojanovic, M. N., Green, E. G., Semova, S., Nikic, D. B., and Landry, D. W. (2003) Cross-Reactive Arrays Based on Three-Way Junctions. *J. Am. Chem. Soc. 125*, 6085−6089.
(34) Reinstein, O., Neves, M. A. D., Saad, M., Boodram, S. N., Lombardo, S., Beckham, S. A., Brouwer, J., Audette, G. F., Groves, P., Wilce, M. C. J., and Johnson, P. E. (2011) Engineering a Structure Switching Mechanism into a Steroid Binding Aptamer and Hydrodynamic Analysis of the Ligand Binding Mechanism. *Biochemistry 50*, 9368−9376.
(35) Neves, M. A. D., Reinstein, O., Saad, M., and Johnson, P. E. (2010) Defining the Secondary Structural Requirements of a Cocaine-Binding Aptamer by a Thermodynamic and Mutation Study. *Biophys. Chem. 153*, 9−16.
(36) Sharma, A. K., and Heemstra, J. M. (2011) Small-Molecule-Dependent Split Aptamer Ligation. *J. Am. Chem. Soc. 133*, 12426−12429.
(37) Sharma, A. K., Kent, A. D., and Heemstra, J. M. (2012) Enzyme-Linked Small-Molecule Detection Using Split Aptamer Ligation. *Anal. Chem. 84*, 6104−6109.
(38) Pei, R., Shen, A., Olah, M. J., Stefanovic, D., Worgall, T., and Stojanovic, M. N. (2009) High-Resolution Cross-Reactive Array for Alkaloids. *Chem. Commun.*, 3193−3195.
(39) Bao, J., Krylova, S. M., Reinstein, O., Johnson, P. E., and Krylov, S. N. (2011) Label-Free Solution-Based Kinetic Study of Aptamer-Small-Molecule Interactions Reveals How Kinetics Control Equilibrium. *Anal. Chem. 83*, 8387−8390.
(40) Spiropulos, N. G., and Heemstra, J. M. (2012) Templating Effect in DNA Proximity Ligation Enables Use of Non-Bioorthogonal Chemistry in Biological Fluids. *Artificial DNA: RNA & XNA 3*, 123−128.
(41) Wiseman, T., Williston, S., Brandts, J. F., and Lin, L.-N. (1989) Rapid Measurement of Binding Constants and Heats of Binding Using a New Titration Calorimeter. *Anal. Biochem. 179*, 131−137.
(42) Turnbull, W. B., and Daranas, A. H. (2003) On the Value of C: Can Low Affinity Systems Be Studied by Isothermal Titration Calorimetry? *J. Am. Chem. Soc. 125*, 14859−14866.
(43) Tellinghuisen, J. (2008) Isothermal Titration Calorimetry at Very Low C. *Anal. Biochem. 373*, 395−397.
(44) Jeener, J., Meier, B. H., Bachmann, P., and Ernst, R. R. (1979) Investigation of Exchange Processes by Two-Dimensional NMR Spectroscopy. *J. Chem. Phys. 71*, 4546−4553.
(45) Macura, S., and Ernst, R. R. (1980) Elucidation of Cross Relaxation in Liquids by Two-Dimensional NMR Spectroscopy. *Mol. Phys. 41*, 95−117.
(46) Piotto, M., Saudek, V., and Sklenar, V. (1992) Gradient-Tailored Excitation for Single-Quantum NMR Spectroscopy of Aqueous Solutions. *J. Biomol. NMR 2*, 661−665.
(47) Delaglio, F., Grzesiek, S., Vuister, G. W., Zhu, G., Pfeifer, J., and Bax, A. (1995) NMRPipe: A Multidimensional Spectral Processing System Based on UNIX Pipes. *J. Biomol. NMR 6*, 277−293.
(48) Franke, D., and Svergun, D. I. (2009) DAMMIF, a Program for Rapid Ab Initio Shape Determination in Small-Angle Scattering. *J. Appl. Crystallogr. 42*, 342−346.
(49) Muhuri, S., Mimura, K., Miyoshi, D., and Sugimoto, N. (2009) Stabilization of Three-Way Junctions of DNA under Molecular Crowding Conditions. *J. Am. Chem. Soc. 131*, 9268−9280.
(50) Fukada, H., and Takahashi, K. (1998) Enthalpy and Heat Capacity Changes for the Proton Dissociation of Various Buffer Components in 0.1 M Potassium Chloride. *Proteins 33*, 159−166.
(51) Feig, A. L. (2009) Studying RNA−RNA and RNA−Protein Interactions by Isothermal Titration Calorimetry. *Methods Enzymol. 468*, 409−422.
(52) Record, M. T., Jr., Anderson, C. F., and Lohman, T. M. (1978) Thermodynamic Analysis of Ion Effects on the Binding and Conformational Equilibria of Proteins and Nucleic Acids: The Roles of Ion Association or Release, Screening, and Ion Effects on Water Activity. *Q. Rev. Biophys. 11*, 103−178.
(53) Sigurskjold, B. W. (2000) Exact Analysis of Competition Ligand Binding by Displacement Isothermal Titration Calorimetry. *Anal. Biochem. 277*, 260−266.
(54) Chaires, J. B. (2008) Calorimetry and Thermodynamics in Drug Design. *Annu. Rev. Biophys. 37*, 135−151.
(55) Spolar, R. S., and Record, M., Jr. (1994) Coupling of Local Folding to Site-Specific Binding of Proteins to DNA. *Science 263*, 777−784.
(56) Kaul, M., Barbieri, C. M., and Pilch, D. S. (2005) Defining the Basis for the Specificity of Aminoglycoside-rRNA Recogntion: A Comparative Study of Drug Binding to the A Sites of *Escherichia coli* and Human rRNA. *J. Mol. Biol. 346*, 119−134.
(57) Kozin, M., and Svergun, D. I. (2001) Automated Matching of High- And Low-Resolution Structural Models. *J. Appl. Crystallogr. 34*, 33−41.